Journal of The Electrochemical Society, **156** (5) K72-K76 (2009)
0013-4651/2009/156(5)/K72/5/$23.00 © The Electrochemical Society

Implantation, Characterization, and Formation Mechanisms of Gold Nanocrystals in TiO_2 Thin Film and Nanowires

Jyh Ming Wu[*,z]

Department of Material Science and Engineering, Feng Chia University, Taichung 40724, Taiwan

Gold (Au) nanocrystals were thermally evaporated and implanted into a TiO_2 film by a two-step vacuum process. In the experiment, two different specimens, as-prepared sample Au/Ti/Si substrate and source material Ti powder were combined. In the first stage, the materials underwent thermal evaporation (at 850°C for the first material and at 1050°C for the second material) under a vacuum pressure of $\sim 10^{-3}$ Torr for 1 h. In the second step, the vacuum system was fed with air and maintained at 760 Torr for 1 h. The air pressure implanted the Au nanoclusters into the TiO_2 film. The process also synthesized TiO_2 nanowires. High-angle annular dark-field imaging by a scanning transmission electron microscope (HAADF/STEM) revealed that the Au nanocrystals (nanoclusters) were highly dispersed in the TiO_2 film and its nanowires. The diameters of the TiO_2 nanowires ranged from 60 to 100 nm, and their lengths were up to 3 μm. High-resolution transmission electron microscopy with energy dispersive X-ray spectroscopy mapping, HAADF/STEM, X-ray photoelectron spectroscopy, and X-ray diffractometry were used to elucidate the formation process of the as-synthesized products. The results indicated that as-synthesized nanowires had been formed by a combination of solid-liquid-solid and vapor-solid mechanisms.
 [DOI: 10.1149/1.3089304]

Manuscript submitted September 18, 2008; revised manuscript received January 30, 2009. Published March 10, 2009.

Ion implantation technologies have been widely used in metallic oxide semiconductor fabrication with solid-state reactions due to their applications in nonlinear optical devices.[1] Today, semiconductor processors use ion implantation for almost all doping in silicon-based devices. However, the implantation process requires an expensive facility and complicated support systems.

TiO_2 is a well-known metal oxide that has been researched for more than 30 years. Haruta[2] demonstrated that Au acts as a catalyst for low-temperature CO oxidation when dispersed as nanoclusters on a TiO_2 matrix. In the present study, a two-step vacuum process with thermal evaporation was employed to implant gold (Au) nanocrystals into a TiO_2 film. This process achieved a large implantation area. In the first step, a ~50 nm film of Au was deposited on a Ti/Si substrate (which had 200 nm of Ti layered on Si), then the as-prepared substrate (Au/Ti/Si) and Ti powder (source material) were thermally annealed under a vacuum pressure of 10^{-3} Torr for 1 h. In the second step, the pressure was switched to 760 Torr by introducing atmospheric air; this pressure was maintained for 1 h. After the experiment, TiO_2 nanowires were found to have grown on the substrate. Also, highly dispersed Au nanocrystals were found implanted within a large area of TiO_2 film; Au nanocrystals were also found both on surfaces and implanted within the TiO_2 nanowires. High-angle annular dark field imaging by a scanning transmission electron microscope (HAADF/STEM) revealed that the TiO_2 film possessed many Au nanocrystals, of which the average size was <10 nm. Moreover, many nanowires, studded with these Au nanocrystals, were found throughout the sample.

We propose this two-step vacuum process to implant Au nanocrystals into TiO_2 film. However, Ti is a refractory material with a high melting point of 1668°C,[3] thus the question is how to synthesize TiO_2 nanowires by a vapor deposition process (thermal evaporation) at a substrate temperature of 850°C. To consider this issue in terms of vapor pressure, note that vapor pressure (p) is generally expressed as[4]

$$\log p = \frac{a}{T} + b \log T + c + d$$

where a, b, c, and d are constants determined by a variety of substances.[5] The vapor pressure of Ti is $\sim 10^{-3}$ Torr at 1577°C, thus fabrication of TiO_2 nanostructures by the vapor-phase method is a challenge. To address this challenge, a previous study reported that a predeposited TiO_2 film can be employed to grow TiO_2 nanowires on activated nucleation sites.[6] These nanowires were synthesized through a vapor-solid (VS) process[7,8] and a vapor-liquid-solid (VLS) process.[9,10] In the present work, an experiment has been designed to clarify the formation mechanism of TiO_2 nanowires. The whole process can be regarded as a combination of solid-liquid-solid (SLS)[11] and VS mechanisms. This work describes how the TiO_2 nanowires formed and how the Au nanocrystals became embedded in the TiO_2 (film) matrix.

Experimental

The experimental setup is similar to the setup of a previous report.[12] Ti powder (1.5 g, purity 99.9%, Alfa Aesar) was used as a source material. A Ti thin film (~200 nm) was predeposited on a Si substrate. An Au film (~50 Å) was then deposited on the Ti/Si substrate. Ti powder was placed in the high-temperature (HT) zone on the upstream side of the graphite boat, while the as-prepared substrate (Au/Ti/Si) was placed in the low-temperature (LT) zone on the downstream side, as shown in Fig. 1. The HT zone was heated by a radio-frequency (350 kHz) heater, while the LT zone was heated by an electrical resistance heater. In the first step, the vacuum system was evacuated down to $\sim 10^{-3}$ Torr. A constant stream of argon (40 sccm, purity: 99.99%) was introduced to the system. The HT zone was heated to 1050°C, while the LT zone was heated to 850°C. At the same time, 0.5 sccm oxygen gas (O_2, purity: 99.99%) was introduced into the quartz reactor. The system was held at these temperatures with a pressure of 10^{-3} Torr for 1 h. In the second step, the vacuum system was switched to 760 Torr by opening the chamber to atmospheric pressure. The system was maintained at this pressure for 1 h. After the process was finished,

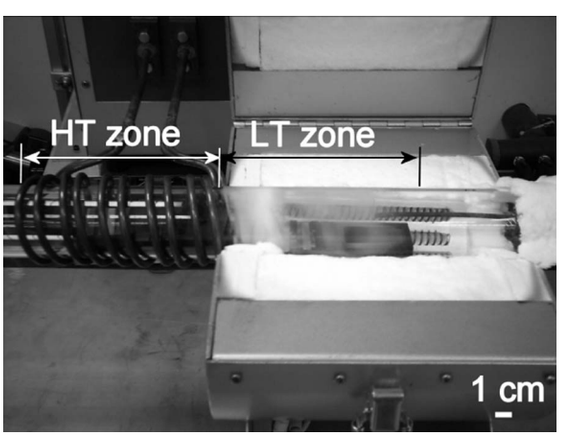

Figure 1. Two-evaporation-zone system.

* Electrochemical Society Active Member.
z E-mail: jmwu@fcu.edu.tw

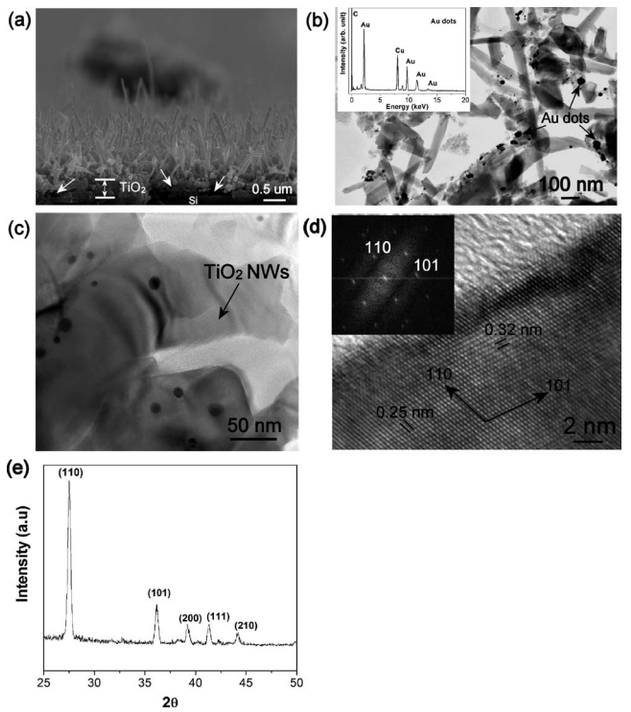

Figure 2. (a) A cross-sectional FESEM image of TiO_2 nanowires grown on TiO_2/Si substrate. Pore formation in TiO_2 film is indicated by white arrows. (b) TEM image: black dots represent Au nanocrystals; inset is the EDS spectrum of Au dots. (c) Cross-sectional TEM image showed that the Au nanocrystals (black inclusions) were embedded in TiO_2 nanowires. (d) HR-TEM image shows the lattice fringe 0.32 nm; SAD pattern is inset, and (e) XRD patterns of as-synthesized nanowires.

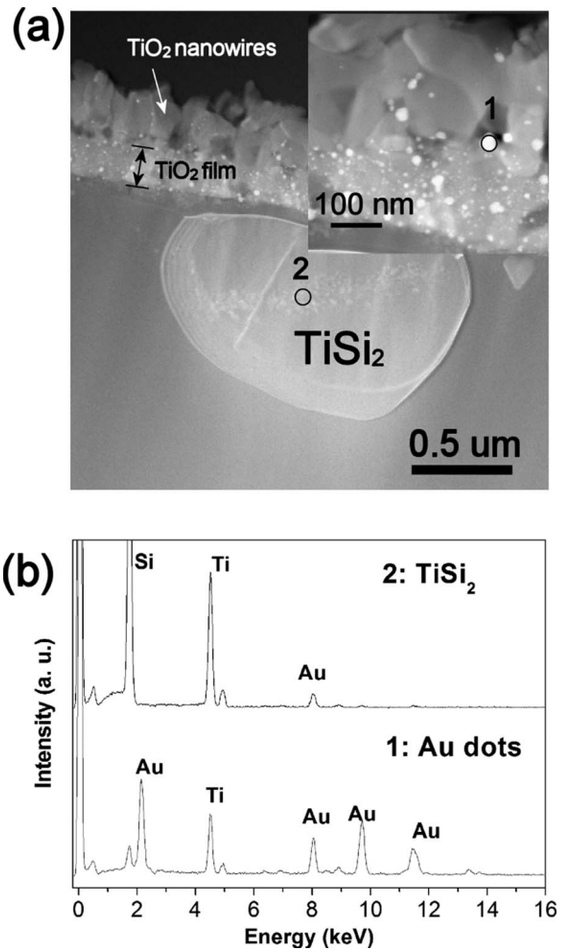

Figure 3. Cross-sectional HAADF/STEM images (a) HAADF image, white dots represent Au nanocrystals; inset image reveals the average size is <10 nm; islandlike microcrystal beneath TiO_2 film is attributed to the $TiSi_2$; (b) EDS spectra from the corresponding marker of 1 (Au nanocrystals) and 2 ($TiSi_2$ microcrystal).

Au nanocrystals were found within the TiO_2 film and nanowires. In addition, it was found that some Au nanocrystals had adhered to the nanowires' surfaces.

The structure of the sample was analyzed with a X-ray diffraction (XRD) Philips PW3710 diffractometer. The as-synthesized products were analyzed with a high-resolution transmission electron microscope [(HRTEM), JEOL JEM-2000FX, operated at 200 kV], a HAADF/STEM, and a field emission scanning electron microscope [(FESEM), JOEL 7000, operated at 10 kV]. The composition of the as-synthesized products was analyzed by energy dispersive X-ray spectroscopy (EDS), which was done with the HRTEM. The samples were analyzed by X-ray photoelectron spectroscopy [(XPS), Perkin-Elmer model PHI600 system] using a single Mg Kα X-ray source (1253.6 eV), which was operated at 250 W.

Results and Discussion

Materials characterization.— Figure 2a shows that TiO_2 nanowires grew on the TiO_2/Si substrate. During the growth process, the predeposited Ti film was transformed to a TiO_2 film when the process temperature reached $\sim$450°C. The processed TiO_2 film exhibits less density and fewer pores (see the white arrows) than the original film had. Figure 2b reveals the randomly distributed positions of the black inclusions that adhered to the surfaces of the TiO_2 nanowires. The transmission electron microscope (TEM) EDS profile indicated that these black inclusions can be attributed to the Au element, as shown in the inset of Fig. 2b. The copper (Cu) and carbon (C) peaks in the EDS spectrum were caused by the carbon-coated grid of the TEM specimen. Although Fig. 2b shows that some Au nanocrystals adhered to the surface of the nanowires, the cross-sectional TEM image in Fig. 2c indicates that some Au inclusions could be embedded in the TiO_2 nanowires. Further clarification should be conducted by the nanowires' cross-sectional TEM observations (i.e., perpendicular to growth axis of the nanowires). Figure 2d, the HRTEM image, reveals an individual TiO_2 nanowire with a clear lattice fringe that has spacings $\sim$0.32 nm wide. The inset in Fig. 2d is a fast Fourier transform (FFT) of the HRTEM image. Comparison of the FFT pattern and the corresponding lattice spacing of TiO_2 confirms that the nanowire grew along the [110] axis. Figure 2e indicates that all as-synthesized nanowires belong to the rutile phase of TiO_2 (JCPDS 21-1276). According to the TEM and scanning electron microscope (SEM) images, although the experiment employed Au as the catalyst for growing the one-dimensional (1D) nanostructures, the Au nanoparticles did not position themselves at the tips of nanowires but rather incorporated themselves throughout the TiO_2 thin film and nanowire. In addition, some Au nanocrystals were found on the nanowires' surfaces.

The HAADF/STEM image reveals that the Au nanocrystals were highly dispersed in the TiO_2 film, as shown in Fig. 3a. The inset image in Fig. 3a shows the Au nanocrystals as white dots because the atomic number (Z) of Au is larger than the atomic numbers of elements such as Ti, Si, and O, and thus Au is heavier than those elements. An EDS spectrum (marked as 1 in the inset of Fig. 3a) in Fig. 3b clearly indicates that the white dots are attributable to the Au component. The single peak of Ti can be ascribed to the TiO_2, which was positioned around the Au dots (details to follow). According to the cross-sectional TEM image, the Au nanocrystals had sizes of <10 nm and were highly dispersed throughout the TiO_2 film. An

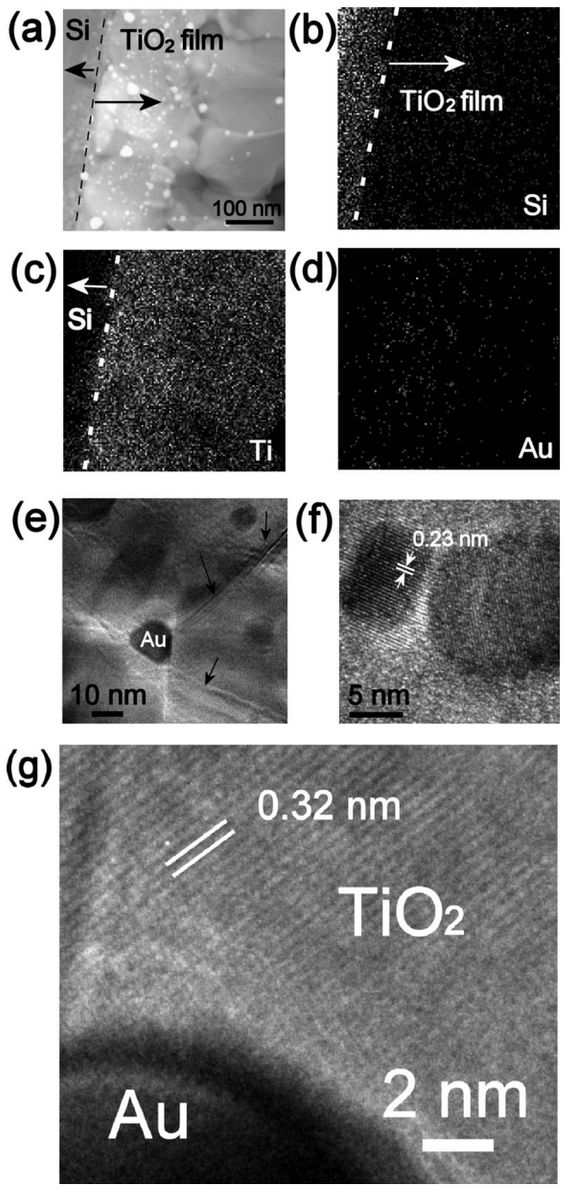

Figure 4. (a) HAADF-STEM image of TiO_2/Si substrate; a dashed line was used to discriminate the Si substrate and the TiO_2 film. (b–d) are corresponding EDS mappings of (b) Si, (c) Ti, and (d) Au. (e) Au nanocrystals incorporated into the TiO_2 film induce the slip band with clear dislocation lines. (f) Au nanocrystals with lattice fringe, and (g) Au nanocrystals contained in TiO_2 film.

islandlike microcrystal of TiSi compound was found beneath the processed TiO_2 film, as shown in Fig. 3a. The EDS spectrum (marked as 2 in Fig. 3a) in Fig. 3b confirmed that the islandlike mass was composed of titanium-silicide (i.e., $TiSi_2$) with a trace of Au. This can be ascribed to the reaction of the predeposited Ti film with the Si substrate at an elevated temperature, which resulted in the precipitation of $TiSi_2$ at the Ti–Si interface.[13] The weak Au peak can be ascribed to diffusion of the Au component into the titanium-silicide compound.

To reveal all elements in the TEM specimen, a dashed line was used in Fig. 4a to discriminate between the Si substrate and the TiO_2 film. The HAADF image in Fig. 4a shows that Au nanocrystals were also implanted in the Si substrate (as shown by the white dots on the left side of the dashed line). The elemental distributions of Si, Ti, and Au were determined by EDS mapping on the as-synthesized TiO_2 film, as shown in Fig. 4b-d. The TEM EDS mapping showed that not only was the TiO_2 film highly permeated with Au nanocrystals, but also that interdiffusion had happened between Ti and Si (as seen in Fig. 4b and c). Figure 4b reveals that the TiO_2 thin film possesses Si inclusions. In contrast, the Ti element was diffused from the TiO_2 thin film to the Si substrate, where it precipitated the Ti–Si compound and formed an islandlike mass (see Fig. 3a). Here, the Si element was obviously dispersed in the TiO_2 thin film. We believe that TiSi compounds existed in the TiO_2 film (of which further details follow). The XRD pattern did not show the TiSi compounds because dense TiO_2 nanowires had grown on the TiO_2 film. However, Au nanocrystals had permeated the TiO_2 film; thus, the slip bands induced dislocation lines that were clearly observable on the HRTEM image, as shown by the black arrow of Fig. 4e. Figure 4f further indicates that the Au nanocrystals exhibited a clear lattice fringe, ~0.23 nm wide, with good crystalline structure. The TiO_2 lattice ~0.32 nm is also shown in Fig. 4g, which confirms that the Ti peak in the EDS spectrum (Fig. 3b, lower curve) can be ascribed to the adjacent TiO_2 that was positioned around the Au dots.

Sputtering was done for XPS investigations; the Ti 2p, Si 2p, O 1s, and C 1s XPS spectra are shown in Fig. 5. The Ti $2p_{1/2}$ peak is consistent with the reported values of TiO_2,[14] as shown in Fig. 5a. Figure 5b reveals a peak at 102.7 eV, which suggests the Si–O[15] bond. In the O 1s spectrum, the peaks at 533 and 530.5 eV can be ascribed to the C–O (or Si–O)[16] and Ti–O[17] bonds, as shown in Fig. 5c. In order to verify that the C–O bonds are not ascribable to atmospheric contamination that might have happened when the sample was exposed to the air, consider Fig. 5d, which shows the C 1s spectrum. The peaks at 288.75, 287, and 285 eV can be ascribed to the CO_3,[18] C–O,[19] and C–C (or C–H)[20,21] bonds, respectively. On the basis of the XPS evaluation, we propose that the following reactions may occur during the formation of as-synthesized products

$$Ti_{(s)} + C_{(s)} + 2O_{2(g)} \rightarrow TiO_{2(s)} + CO_{2(g)}$$

$$\Delta G_1 = -1090 \text{ kJ/mole} \quad [1]$$

$$2H_2O_{(g)} + 3C_{(s)} + O_{2(g)} \rightarrow C_2H_4O_{2(g)} + CO_{2(g)}$$

$$\Delta G_2 = -203 \text{ kJ/mole} \quad [2]$$

$$C_2H_4O_{2(g)} + 2O_{2(g)} \rightarrow 2CO_{2(g)} + 2H_2O_{(g)}$$

$$\Delta G_3 = -589 \text{ kJ/mole} \quad [3]$$

$$Ti_{(s)} + 2Si_{(s)} \rightarrow TiSi_{2(s)}$$

$$\Delta G_4 = -176 \text{ kJ/mole} \quad [4]$$

$$TiSi_{2(s)} + O_{2(g)} \rightarrow Ti_{(g)} + 2SiO_{(g)}$$

$$\Delta G_5 = -1635 \text{ kJ/mole} \quad [5]$$

These reaction routes are considered to be spontaneous reactions because they all have negative Gibbs free energy, which results in the formation of as-synthesized products. For Eq. 1, the sample was placed on the graphite boat; therefore the carbon reacted with O_2 species to produce CO_2 by-products. In the context of Eq. 2, recall that water vapor is comprised of H_2O and O_2 species; at a temperature of 1050°C, these species chemically reacted with carbon and oxygen and then produced $C_2H_4O_2$ with CO_2. Thus, the XPS spectrum in O 1s and C 1s showed the C–H, C–C, and C–O bonds. When $C_2H_4O_2$ gas was exposed to the oxygen species at 1050°C, the $C_2H_4O_2$ disassociated into CO_2 and H_2O, accompanied by a combustion heat process.[22] Equation 3 specifies how this reaction releases a great deal of heat. This reaction enhanced the Ti powder to become a Ti vapor source from which TiO_2 nanowires grew. At an elevated temperature, the predeposited Ti film reacted with the Si substrate to produce the $TiSi_2$ phase, as indicated by Eq. 4.[13] This

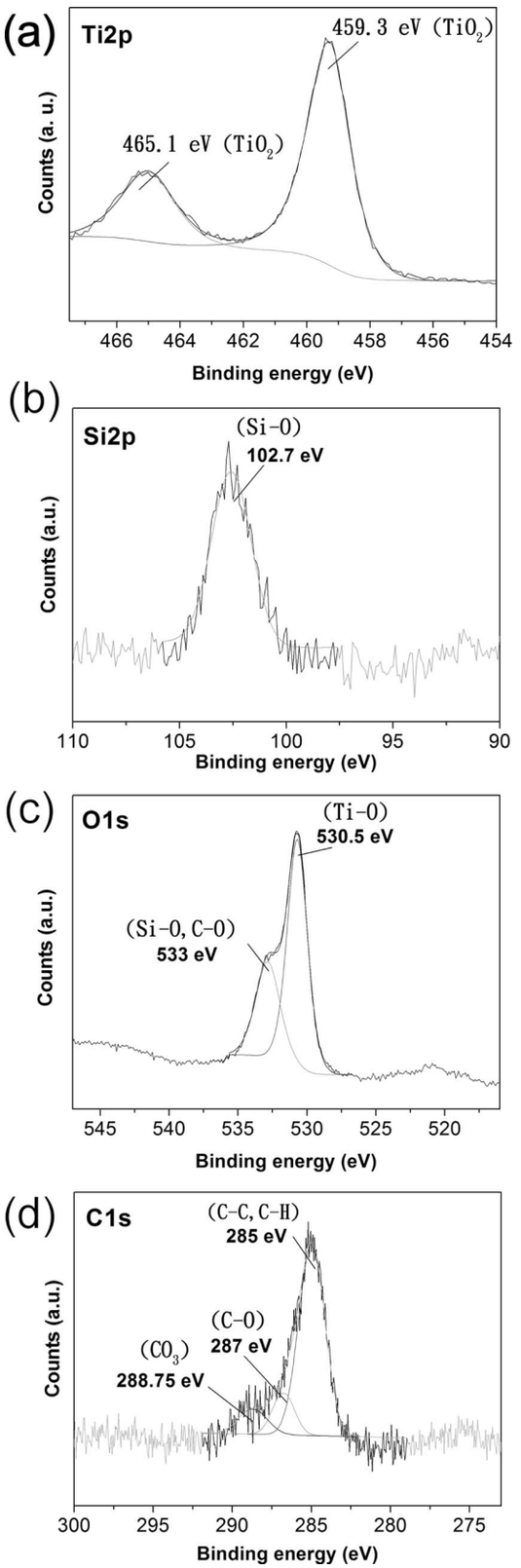

Figure 5. XPS spectra: (a) Ti 2p, (b) Si 2p, (c) O 1s, (d) C 1s.

explains the fact that the TiSi compounds from TiO_2 film were detectable by TEM EDS. Equation 5 further indicates that the $TiSi_2$ phase was strongly dissociated into Ti and SiO (or SiO_x) in an ambient oxygen atmosphere. The SiO_x species remained in the TiO_2 film. Accordingly, the Si–O bond was found in the Si 2p region of the XPS spectrum. This may explain why the TiO_2 film displayed a rich Si concentration, as shown in the TEM EDS mapping in Fig. 4b.

Formation mechanisms.— Because the control samples without Ti powder and TiO_2 film did not synthesize any TiO_2 nanowires,[12] the Ti powder and $TiSi_2$ (within the TiO_2 film) were considered to have served as Ti species for constructing TiO_2 nanowires. Accordingly, the Ti species (solute) was generated either from the $TiSi_2$ in the TiO_2 film or from the Ti vapor that had been generated from the Ti powder in the HT (1050°C) zone. As the Ti species were provided from TiSi (i.e., $TiSi_2$) compounds in TiO_2 film, the Ti solutes diffused from $TiSi_2$ to Au-rich TiAu alloy (liquid droplets), so that a liquid-solid interface was formed, at which the Ti solutes were continuously absorbed in the liquid phase of the Au-rich TiAu nanoclusters[6] until the solution became supersaturated.[23] Then, the liquid-solid interface of the TiAu alloy precipitated the solid phase of TiO_2. Because the solutes of Ti were continuously diffused from the TiO_2 film, eventually the TiO_2 film became porous (see the cross-sectional SEM image in Fig. 2a). However, as described in Eq. 5, one of the reactions for solid-state diffusion under a large thermodynamic driving force occurred, resulting in a dissociation of $TiSi_2$ into Ti and SiO (or SiO_x) species. Each nanowire began when some Ti vapor condensed on a small area of the film surface, changing the geometry. Subsequently, more and more of the Ti species solidified onto the TiO_2 nucleation site, thus constructing the nanowire. The growth happened through a solid-liquid-solid process, so the formation of TiO_2 nanowires involved an SLS mechanism.

As mentioned above, the Ti species generated from Ti powder in the HT zone may have also provided material for TiO_2 nanowires. Previous work found that Au and TiO_2 films can act as catalysts and as active sites (nucleation sites) that grow TiO_2 nanowires by VLS[12] and VS[6] mechanisms. Extrapolating from a typical VLS mechanism, one would expect the reactant species (i.e., Ti vapor) to be transferred from the HT zone and to condense on the Au liquid droplets in the LT zone, subsequently precipitating 1D nanowires from Au catalyst heads. The previous nanowires were shaped like matchsticks because the catalyst heads (melting state) were pulled to the tips of the nanowires. However, in this work, the Au did not act as a catalyst for growing 1D nanostructures; it acted as a metal source for implantation. We suggest that the Ti powder was highly oxidized with low vapor pressure at a temperature of 1050°C (in the HT zone). The low vapor pressure of Ti did not provide enough gas to the Au catalyst to precipitate 1D nanostructures. Therefore, matchstick-shaped nanowires did not form because the VLS was not satisfied in time. In previous research,[12] the as-prepared TiO_2 film was provided with high surface energy sites, which enabled the finite Ti gas to accumulate on these sites to reduce the total free energy;[24] therefore the most thermally stable crystalline plane of (110) TiO_2 was present and the 1D morphology was formed.[25] This is a typical VS mechanism that has been demonstrated in detail in previous studies.[6] However, during the crystal growth process, vapor phase Ti appeared from Ti powder in the HT zone, thus the growth of TiO_2 nanowires can still be considered to involve a VS mechanism. On the basis of the analysis above, the whole process can be regarded as a combination of SLS and VS mechanisms.

This research has investigated how the Au nanocrystals became highly scattered and distributed throughout the TiO_2 film and nanowires. A schematic diagram in Fig. 6 depicts the formation process. Figure 6a shows that, at a substrate temperature of ~850°C, the molten Au clusters formed round shapes throughout the entire area of the TiO_2 film. For the VS mechanism, the Ti vapors from the Ti powder in the HT zone provided matter for the TiO_2 nanowires. In contrast, for the SLS mechanism, the Ti species were provided from the $TiSi_2$ phase of the TiO_2 film. The SLS mechanism formed the pores in the TiO_2 film by constructing TiO_2 nanowires. Additionally, the growth process was controlled by two different pressure levels

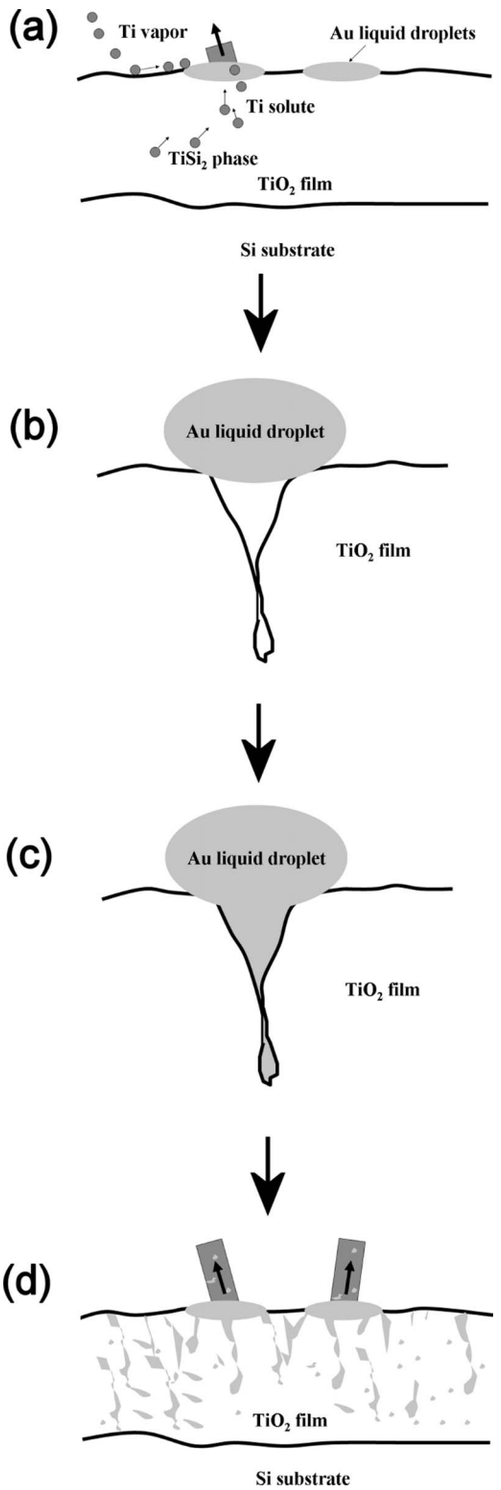

Figure 6. (a–d) Implantation of Au nanocrystals in TiO_2 film and its nanowires; see the text for details.

for 1 h each: 10^{-3} Torr for step 1, and 760 Torr for step 2. For the second step, the pressure of the vacuum system suddenly increased to 760 Torr because the valve of the chamber was opened to atmospheric pressure; a pressure difference was exhibited between the inside of the quartz reactor and the porous TiO_2 film. Specifically, two pressures appear at the transition point between 10^{-3} and 760 Torr. In response to the influx of air, the molten Au nanoclusters permeated into the porous TiO_2 film, as shown in Fig. 6b and c. Additionally, the TiO_2 film and nanowires had many densely packed oxygen vacancies,[8] which were the active nucleation sites for Au nanoclusters on the $TiO_2(110)$ surfaces at all temperatures.[26] The nucleation and growth processes of as-synthesized products caused wide scattering of the Au nanocrystals throughout the TiO_2 film and nanowires, as shown in Fig. 6d. This phenomenon explains why the Au nanoclusters were highly scattered in the TiO_2 film and its nanowires.

Conclusion

Au nanocrystals were implanted into TiO_2 films. XPS revealed C–C, C–O, and C–H bonds, which suggested that C, H_2O, and O had participated in the reaction. SLS and VS mechanisms have been suggested as having dominated the growth of TiO_2 nanowires. The Ti species were provided from the $TiSi_2$ phase of the TiO_2 film and from the Ti powder from the HT zone. Two pressures appeared at the transition point between 10^{-3} and 760 Torr. In response to the influx of air, the molten Au nanoclusters permeated into the porous TiO_2 film. The porous TiO_2 film had many oxygen vacancies that acted as active nucleation sites for Au nanoclusters on the $TiO_2(110)$ surface. This work has clarified the formation mechanisms of TiO_2 nanowires and has reported on a process for large-area Au implantation.

Acknowledgments

The authors thank the National Science Council of the Republic of China for financially supporting this research under contract no. NSC 96-2221-E-035-058.

Feng Chia University assisted in meeting the publication costs of this article.

References

1. A. Meldrum, *Adv. Mater. (Weinheim, Ger.)*, **13**, 1431 (2001).
2. M. Haruta, *J. Catal.*, **115**, 301 (1989).
3. J. L. Murray, *Phase Diagrams of Binary Titanium Alloys*, ASM, Metals Park, OH (1987).
4. R. A. Swalin, *Thermodynamics of Solids*, 2nd ed., John Wiley & Sons, Inc., Hoboken, NJ (1972).
5. O. Kubaschewski, C. B. Alcock, and P. J. Spencer, *Materials Thermochemistry*, 6th ed., Pergamon Press, New York (1993).
6. J. M. Wu, H. C. Shih, and W. T. Wu, *Nanotechnology*, **17**, 105 (2006).
7. P. Yang and C. M. Lieber, *J. Mater. Res.*, **12**, 2981 (1997).
8. J. M. Wu, H. C. Shih, W. T. Wu, Y. K. Tseng, and I. C. Chen, *J. Cryst. Growth*, **281**, 384 (2005).
9. R. S. Wagner and W. C. Ellis, *Appl. Phys. Lett.*, **4**, 89 (1964).
10. J. M. Wu, H. C. Shih, and W. T. Wu, *Chem. Phys. Lett.*, **413**, 490 (2005).
11. H. F. Yan, Y. I. Xing, Q. L. Hang, D. P. Yu, Y. P. Wang, J. Xu, Z. H. Xi, and S. Q. Feng, *Chem. Phys. Lett.*, **323**, 224 (2000).
12. J. M. Wu, W. T. Wu, and H. C. Shih, *J. Electrochem. Soc.*, **152**, G613 (2005).
13. J. M. Wu, *J. Phys. Chem. C*, **112**, 13192 (2008).
14. U. Diebold and T. E. Madey, *Surf. Sci. Spectra*, **4**, 227 (1998).
15. B. A. De Angelis, C. Rizzo, S. Contarini, and S. P. Howlett, *Appl. Surf. Sci.*, **51**, 177 (1991).
16. J. M. Martin, L. Vovelle, M. Bou, and T. L. Mogne, *Appl. Surf. Sci.*, **47**, 149 (1991).
17. B. F. Dzhurinskii, D. Gati, N. P. Sergushin, V. I. Nefedov, and Y. V. Salyn, *Russ. J. Inorg. Chem.*, **20**, 2307 (1975).
18. C. H. Shan and W. Kowbel, *Carbon*, **28**, 287 (1990).
19. D. Rats, L. Vandenbulcke, R. Herbin, R. Benoit, R. Erre, V. Serin, and J. Sevely, *Thin Solid Films*, **270**, 177 (1995).
20. A. Hamwi, C. Latouche, J. Dupuis, R. Benoit, and V. Marchand, *J. Phys. Chem. Solids*, **57**, 991 (1996).
21. P. Brault, P. Ranson, H. Estrade-Szwarckopf, and B. Rousseau, *J. Appl. Phys.*, **68**, 1702 (1990).
22. *CRC Handbook of Chemistry and Physics (on CD-ROM)*, Section 5, p. 5-61, Taylor & Francis, New York.
23. J. C. Lee, K. S. Park, T. G. Kim, H. J. Choi, and Y. M. Sung, *Nanotechnology*, **17**, 4317 (2006).
24. D. A. Porter and K. E. Easterling, *Phase Transformations in Metals and Alloys*, 2nd ed., p. 193, Nelson Thornes, Cheltenham (2001).
25. V. E. Henrich and P. A. Cox, *The Surface Science of Metal Oxides*, p. 43, Cambridge University Press, New York (1994).
26. E. Wahlström, N. Lopez, R. Schaub, P. Thostrup, A. Rønnau, C. Africh, E. Lægsgaard, J. K. Nørskov, and F. Besenbacher, *Phys. Rev. Lett.*, **90**, 026101 (2003).